Journal of Applied Electrochemistry (2022) 52:1459–1467
https://doi.org/10.1007/s10800-022-01724-8

RESEARCH ARTICLE

Effect of a Cu_2O buffer layer on the efficiency in p-Cu_2O/ZnO hetero-junction photovoltaics using electrochemical deposition processing

Leo Chau-Kuang Liau[1] · **Cheng-Hao Tang**[1]

Received: 6 January 2022 / Accepted: 3 June 2022 / Published online: 20 June 2022

Abstract

Herein, we designed and fabricated photovoltaic (PV) devices with optimal efficiency of Cu_2O buffer layers (p-Cu_2O/n-Cu_2O/ZnO and p-Cu_2O/p^--Cu_2O/ZnO) through electrochemical deposition (ECD) processing. PV devices with two types of buffer layers, n-Cu_2O and p^--Cu_2O, were produced by ECD and consisted of a layer of nanorod ZnO on ITO, an n-Cu_2O or a p^--Cu_2O buffer layer, a p-Cu_2O layer, and a sputtered Ag layer. Results revealed that the interface between the ZnO film and the Cu_2O buffer, and thickness of the buffer layer were crucial factors to affect PV device performance. The nanorod structure of ZnO transformed into a flake structure during the ECD of n-Cu_2O on ZnO. However, ZnO retained the same morphology during the ECD of p^--Cu_2O on ZnO. The optimal thicknesses of the Cu_2O buffer in the PV device were obtained to enhance the PV efficiency from 0.046 (p-Cu_2O/ZnO) to 0.17% (p-Cu_2O/p^--Cu_2O/ZnO). The p-Cu_2O/ZnO PV performance was improved through the fabrication and incorporation of Cu_2O buffers.

Graphical abstract

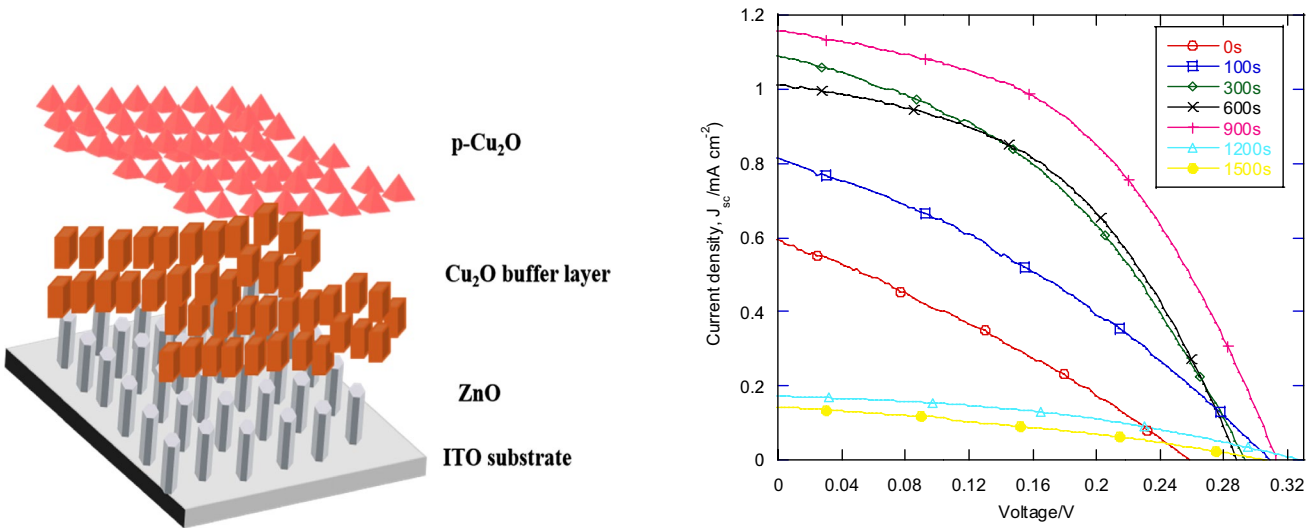

Keywords Nanord ZnO · Solar cell · Cu_2O buffer · Electrochemical deposition

✉ Leo Chau-Kuang Liau
lckliau@saturn.yzu.edu.tw

[1] Department of Chemical Engineering and Materials Science, Yuan Ze University, Taoyang 32003, Taiwan

1 Introduction

A challenge in the field of photovoltaic (PV) technology is the development of high performance PV devices using low-cost and environmentally friendly materials, and processing methods. Zinc oxide (ZnO) and cuprous oxide (Cu_2O), which are abundant and nontoxic, are promising candidates for use in various optoelectronic applications, including in PVs [1, 2], photocatalysis [3], water splitting [4, 5], and sensors [6]. However, the further development of the applications is limited by the efficiency and stability of Cu_2O-based devices. The performance of such devices can be optimized through improvements to their design and fabrication.

PV devices generally consist of p–n junctions and exist as either homo-junction or hetero-junction structures. Cu_2O-based PVs have been recently reviewed and reported in literature [1, 2]. Through the combination of n- and p-Cu_2O semiconductors, p–n-Cu_2O homo-junction PV devices were investigated [7–9]. Although homo-junction devices are considered superior to hetero-junction devices as junction interfaces, homo-junction PVs exhibited a lower efficiency. The hetero-junction structure of Cu_2O-based PV devices has been demonstrated to substantially improve PV performance. Cu_2O-based PV devices with n-ZnO and p-Cu_2O have been designed and fabricated recently [10–27]. The junction interface of these films has been established as an essential factor to influence the PV performance. Furthermore, the properties of ZnO and Cu_2O films have been examined and shown to affect PV performance.

The use of ZnO and Cu_2O to produce PV devices has been extensively studied. Various approaches for the fabrication of ZnO and Cu_2O films have been proposed, such as chemical vapor deposition [10, 11], sputtering [12–24], thermal oxidation [15, 16], and electrochemical deposition (ECD) [17–27]. The properties of ZnO and Cu_2O films (e.g., crystallinity, morphology, and conductivity) and ZnO/Cu_2O interface are affected by the fabrication method. Although high-quality ZnO and Cu_2O films are produced under high-temperature processing conditions, the production cost of the PV devices cannot be down. As for low-temperature processing, ECD is a popular, simple, and low-cost method for ZnO and Cu_2O film fabrication.

Fabricating p-Cu_2O/n-ZnO films through ECD is a popular approach for PV production. The quality of ZnO and Cu_2O films can be controlled by the selection of ZnO amd Cu_2O types through ECD processing [17–27]. Numerous types of ZnO nano-structures, such as nano-wires, rods, and tubes, can be prepared using various ECD techniques. ECD processing of Cu_2O on ZnO films has been extensively explored in investigating the properties of the Cu_2O/ZnO films in the studies. Device performance can be improved through the design of specific ZnO nanostructures due to the particular properties that each structure exhibits at the interface. However, defect formation at the ZnO/Cu_2O interface caused current leakage and electron–hole recombination, which occurred in the defect region, further resulting in poor device performance.

Junction damage at the Cu_2O/ZnO interface can be circumvented by designing a buffer layer between the interfaces [28–36]. A ZnO buffer layer was designed and fabricated between a Cu_2O and an Al-doped ZnO layer to alter p–n junction behavior [30]. A p-Cu_2O buffer layer was fabricated between a ZnO and a P^+-Cu_2O layer to increase free electron generation and to prevent electron–hole recombination [31, 32]. Various layers of buffers, including those made of CdS [33, 34], GaP [35], and ZnOS [36], were studied for use in Cu_2O/ZnO PV devices. These buffer layers in the device served as an energy barrier to prevent current leakage in the p–n junction, thus increasing the V_{oc}. The J_{sc} of the device also increased, which was attributed to a reduction in the occurrence of electron–hole recombination as a result of the presence of the buffer layers. Taken together, these findings demonstrate the importance of preventing ZnO/Cu_2O junction defects during ECD processing under the goal of enhancing PV performance. Herein, a Cu_2O buffer layer was design and fabricated in a p-Cu_2O/ZnO PV device through ECD processing. Two types of buffer layers, n- Cu_2O and p^--Cu_2O, were examined and their effects on the PV performance were determined. The influence of the buffer layer on the PV device was evaluated using data obtained by solar simulation. The optimal fabrication method of the Cu_2O buffer for the device was identified; furthermore, the improvement of the device performance in the presence of the Cu_2O buffer is discussed.

2 Experimental section

2.1 ECD of ZnO and Cu_2O films

Several ECD solutions were prepared for the fabrication of ZnO, n-Cu_2O, p^--Cu_2O, and p-Cu_2O films. Zinc nitrate $Zn(NO_3)_2$ solutions (pH = 5) at 0.01 M thoroughly stirred at 70 °C for 60 min. were prepared for ECD of the ZnO film. The ECD solution of n-Cu_2O was prepared using copper (II) nitrate ($Cu(NO_3)_2$) solutions at 0.01 M and pH = 5. The solutions used for p^--Cu_2O and p-Cu_2O deposition were mixed of copper (II) sulfate ($Cu(SO_4)$) at 0.02 M and lactic acid solution at pH = 9 and 11, respectively, by the adjustment of NaOH. The deposition of the ECD films used an electrochemical analyzer type 6081 C with a three-electrode cell provided by CH Instruments in the ECD system. The deposited films were carried out using indium doped tin oxide

(ITO) as the working electrodes. ITO glass is a commercial product and was purchased from AimCore Technology Co., Taiwan. The counter electrode consisted of platinum and the reference electrode was an Ag/AgCl electrode in 3 M KCl solution. The potential value of the reference Ag/AgCl vs NHE is 0.198 V. The temperature of the deposition bath was maintained at 70 °C for the production of all the ECD films. After the deposition processing was completed, the properties of the fabricated ECD films were further characterized.

2.2 Fabrication of p-Cu_2O/ Cu_2O buffer/ZnO devices

The schematic plot of the p-Cu_2O/Cu_2O buffer/ZnO device is shown in Fig. 1. Two kinds of Cu_2O buffer layers, n-Cu_2O and p^--Cu_2O, were designed and fabricated in the PV device. The PV device was fabricated through ECD processing. The first step of the device fabrication was to deposit ZnO film on ITO through ECD processing by setting the potential at − 1.0 V. After ECD, the ZnO film was thermally treated using rapid thermal annealing at 300 °C. The Cu_2O buffer layer, either n-Cu_2O or p^--Cu_2O, was then deposited on top of the annealed ZnO film by setting potential at − 0.02 V and − 0.4 V, respectively. After the deposition of the buffer layer, p-Cu_2O was deposited on the buffer layer. Ag film was sputtered on the p-Cu_2O film as the electrode in the device. After the PV devices were produced through the ECD processing, the device performance was further evaluated by analytical measurements.

2.3 Characterization of ECD films and PV devices

Several analytical instruments were used to determine the properties of the deposited ECD films. The crystal structure of the produced ECD samples was measured by X-ray Diffraction (XRD, SHIMADZU XRD-6000). The morphologies of the ECD samples were illustrated by SEM (HITACHI S-3000H). The semiconductor characteristics of the prepared PV devices were analyzed by current–voltage (I–V) measurements. Electronic characteristics of the Cu_2O samples, produced by ECD processing, were estimated using *I–V* curves of the sample films, and were measured using a SourceMeter (Keithley model 2400). The photovoltaic devices were carried out the measurements of the cell efficiency tests, utilizing a solar cell evaluation system (180 W Solar Simulation equipment, model YSS-50 provided by Yamashita Denso Corp.).

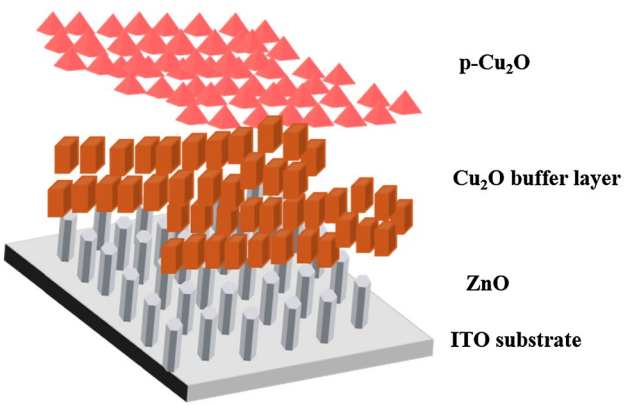

Fig. 1 Plot of the layer structure for the Cu_2O-based PV device

3 Results

3.1 Characterization of ZnO and Cu_2O

The crystal structure of the ECD films was characterized through XRD analysis as shown in Fig. 2a. An XRD pattern with a significant peak at 34.4° (002) and minor peaks at 31.7° (100), 36.2° (101), 47.2° (101), 62.8° (103), and 72.5° (004) was observed for the ZnO film. The pattern corresponds to the hexagonal structure of ZnO crystals (JCPDS, no. 89-0510). The peaks at 29.2° (110), 36.4° (111), 42.3° (200), 62.0° (220), and 73.2° (311), correspond to the cubic crystal structure of Cu_2O (JCPDS, no. 05-0667). An XRD pattern with significant peaks at 34.4° (ZnO) and 36.4° (Cu_2O) exhibits a combination of the peaks of ZnO and Cu_2O and corresponds to the Cu_2O/ZnO structure. The sizes of ZnO and Cu_2O crystals were estimated through the use of XRD patterns and the Scherrer equation to be 48 nm and 54 nm, respectively. The crystal structures resulting from the fabrication of the ECD films are consistent with those reported in literature [6, 9].

The morphologies of the ZnO, Cu_2O, and Cu_2O/ZnO films were analyzed using SEM as shown in Fig. 2. The ZnO particles were rod-shaped, with diameters of 450 nm and heights of 500 nm (Fig. 2b). The ZnO film was employed as the bottom layer of the PV device. Figure 2c demonstrates that the Cu_2O particles produced through ECD on ITO were pyramid-shaped, with lengths of 1 µm. By contrast, the Cu_2O particles, deposited on ZnO, were cube-shaped and had larger edge lengths of 1.2 µm, as shown in Fig. 2d. This indicates that the morphological formation of the deposited Cu_2O is affected by the presence of ZnO. Details on the properties of the ECD films of ZnO and Cu_2O, can be found in our previous studies [37, 38].

3.2 Characterization of Cu_2O buffers and ZnO films

Three types of Cu^{2+} precursors were evaluated for use in the fabrication of Cu_2O buffer layers on ZnO films through ECD. The first precursor, a copper acetate solution, was used to deposit Cu_2O onto the ZnO film. Dendritic particles of n-Cu_2O that formed on ITO in the absence of ZnO presented

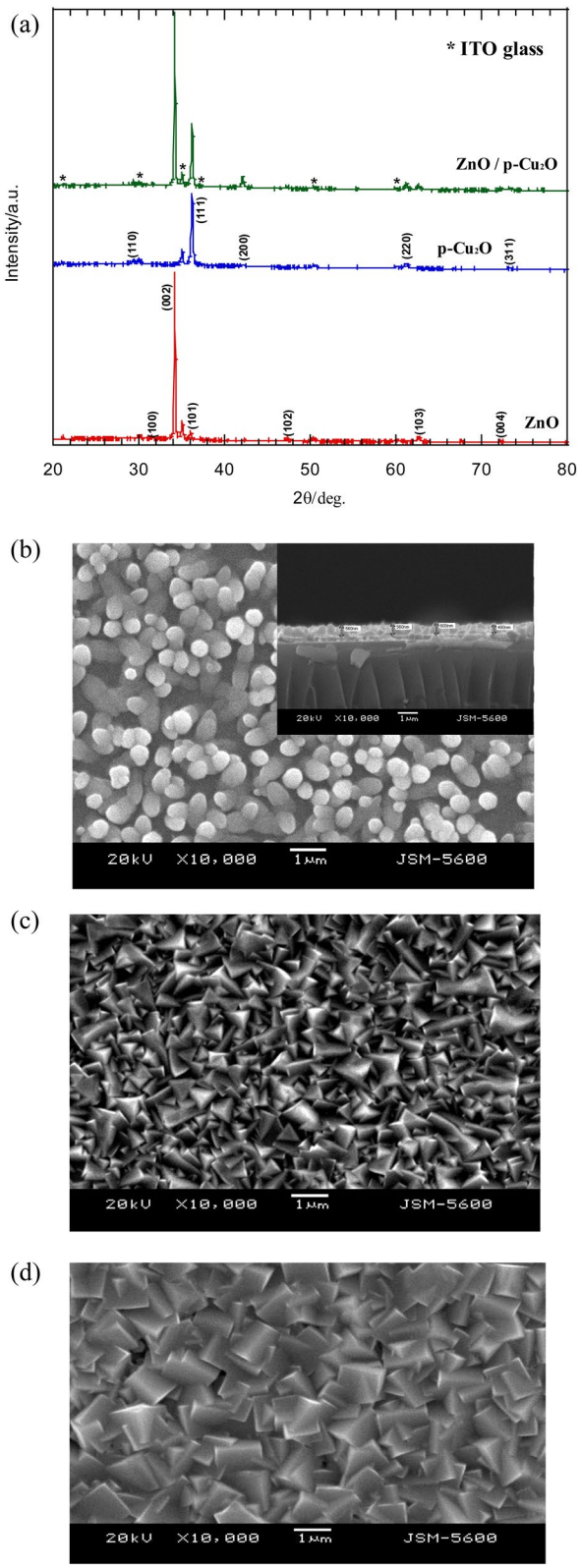

Fig. 2 **a** XRD patterns, and SEM images of **b** ZnO, **c** p-Cu_2O, and **d** p-Cu_2O/ZnO films prepared using ECD processing

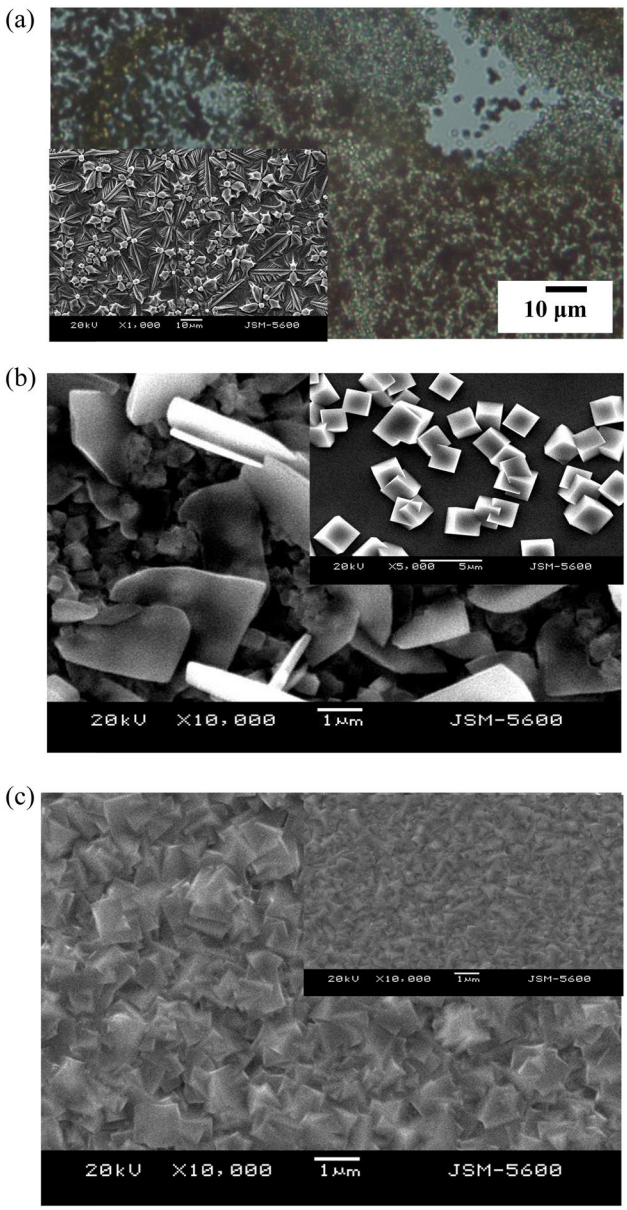

Fig. 3 SEM images of ECD using **a** copper acetate, **b** copper nitrate, and **c** copper sulfate solutions as precursors to deposit Cu_2O particles on ZnO film

in the inset of Fig. 3a. However, when Cu_2O was deposited on top of the ZnO film, the ZnO film was damaged. Some areas on the ZnO film were removed from the substrate during the ECD process (Fig. 3a). Although Cu_2O can be fabricated using copper acetate solution as the precursor, the deposition of Cu_2O on ZnO resulted in the formation of defects on the ZnO film. This ECD process for the fabrication of n-Cu_2O as a buffer layer for PV devices was not further considered.

Use of the second precursor, a $CuNO_3$ solution (pH = 5) resulted in the deposition of cubic particles onto ITO, as

shown in the inset of Fig. 3b [37]. However, when Cu_2O was deposited on the ZnO film, the rod structure of ZnO film transformed to a flake structure. A mixture of small cubic Cu_2O structures and flake-like ZnO structures was observed (Fig. 3b). Unlike the film obtained using the copper acetate solution, the Cu_2O/ZnO film obtained using the $CuNO_3$ solution remained intact. Use of the third precursor, a $CuSO_4$ solution (pH = 9), resulted in the deposition of pyramid-like particles on ITO as presented in the inset of Fig. 3c and p^--Cu_2O semiconductor was reported in literature [6]. When p^--Cu_2O was deposited on the ZnO film, the ECD particles became cube-shaped (Fig. 3c). The p^--Cu_2O/ZnO film was formed without the ZnO film sustaining any damage. Based on the results, n-Cu_2O or p^--Cu_2O were considered potential buffer layers for the fabrication of the present PV devices.

3.3 Multi-layer PV device performance

Two types of multi-layer PV devices were designed and fabricated using ECD. The first type consisted of an n-Cu_2O buffer layer between p-Cu_2O and ZnO films (p-Cu_2O/n-Cu_2O/ZnO). The thickness of the n-Cu_2O layer was controlled through the use of varying deposition periods. The PV parameters of the device, including the short circuit current (J_{sc}), open circuit voltage (V_{oc}), fill factor (FF), and efficiency (η), were evaluated using solar simulation data (Fig. 4a). The PV parameters of the p-Cu_2O/ZnO device without n-Cu_2O were 0.6 mA cm^{-2} (J_{sc}), 0.26 V (V_{oc}), 0.3 (FF), and 0.046% (η), as listed in Table 1a. When the deposition period was set at 100 s, the efficiency of the p-Cu_2O/n-Cu_2O/ZnO device became poor ($\eta = 0.032\%$), compared with that of the p-Cu_2O/ZnO device. Although the J_{sc} rose, a corresponding reduction in the V_{oc} led to poor device performance. One possible reason for this is the formation of flake-like ZnO structures formation during the ECD of n-Cu_2O (Fig. 3b). A series current leakage at the Cu_2O/ZnO interface in the device may have resulted according to current–voltage (*I–V*) curves, as shown in Fig. 4b. At a deposition of 300 s, device efficiency improved ($\eta = 0.13\%$) and maximum PV parameters were noted (Table 1a). A further increase in the deposition period to 600 s did not result in an improvement in device performance. Overall, the results suggest that the thickness of the n-Cu_2O layer strongly affects PV device performance.

The second PV device consisted of a p^--Cu_2O buffer layer between p-Cu_2O and ZnO films (p-Cu_2O/p^--Cu_2O/ZnO). The PV performance of the p-Cu_2O/p^--Cu_2O/ZnO devices under varying deposition periods of the p^--Cu_2O were evaluated using solar simulation data. Figure 5a presents the *I–V* curves for devices fabricated under deposition periods between 0 and 1500 s. The PV parameters of the devices were determined using the *I–V* data (Table 1b). The device efficiencies appear to be strongly influenced

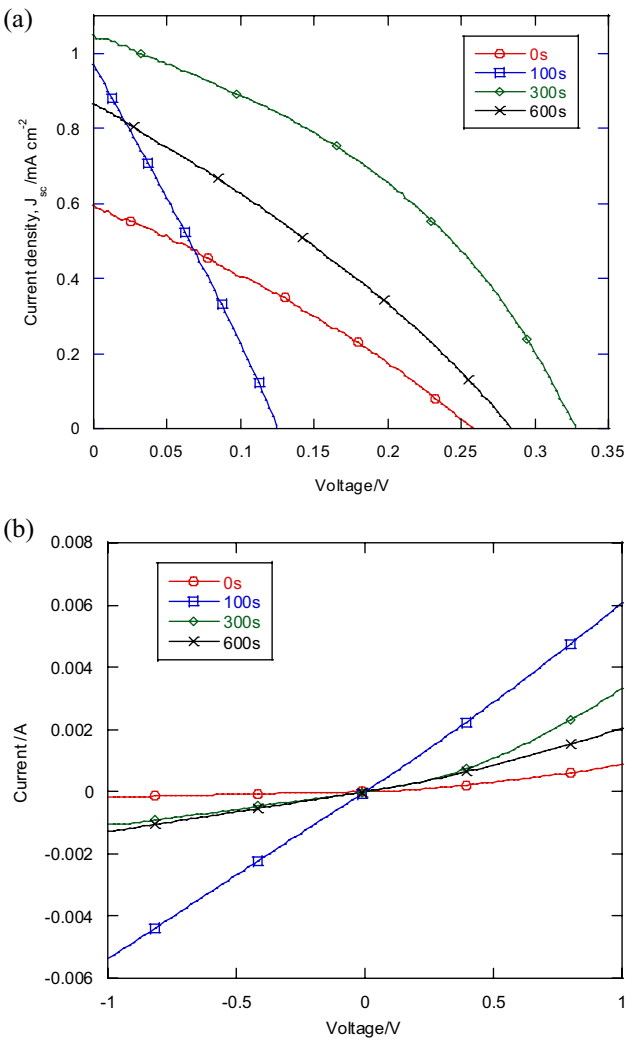

Fig. 4 Various deposition periods of n-Cu_2O in p-Cu_2O/n-Cu_2O/ZnO PV devices for **a** solar simulation and **b** dark *I–V* curve measurements

by J_{sc} for all deposition periods of p^--Cu_2O. The p-Cu_2O/p^--Cu_2O/ZnO devices with p^--Cu_2O deposited between 100 and 900 s performed better than the device without p^--Cu_2O (0 s). For example, the PV device in the 100 s case exhibited a higher PV efficiency (0.083%) than that in 0 s case (0.046%). This suggests that the presence of a thin p^--Cu_2O layer can enhance device performance. The optimal device efficiency ($\eta = 0.17\%$) was found under a 900 s deposition period and corresponded to the highest J_{sc} among all cases. However, PV efficiency decreased when the deposition period of p^--Cu_2O was longer than 900 s, mainly due to the reduction in J_{sc}. The dark *I–V* distribution of the devices revealed that the devices exhibited poor diode performance (Fig. 5b). The results indicate that the thickness of the p^--Cu_2O layer in a PV device is critical for PV performance.

Table 1 PV parameters for various deposition periods of (a) n-Cu_2O in p-Cu_2O/n-Cu_2O/ZnO and (b) p^--Cu_2O in p-Cu_2O/p^--Cu_2O/ZnO devices obtained under AM1.5 illumination

(a)

Time/s	0	100	300	600
V_{oc}/V	0.26	0.125	0.327	0.282
J_{sc}/mA cm^{-2}	0.60	0.95	1.04	0.86
FF	0.30	0.27	0.38	0.3
η/%	0.046	0.032	0.13	0.073

(b)

Time/s	0	100	300	600	900	1200	1500
V_{oc}/V	0.26	0.31	0.29	0.29	0.31	0.33	0.31
J_{sc}/mA cm^{-2}	0.60	0.81	1.09	1.01	1.16	0.173	0.143
FF/-	0.30	0.33	0.41	0.47	0.47	0.39	0.33
η/%	0.046	0.083	0.13	0.135	0.17	0.022	0.014

4 Discussion

The design of a buffer layer, such as n-Cu_2O and p^--Cu_2O, for incorporation into p-Cu_2O/ZnO devices can greatly affect device performance. When thin n-Cu_2O and p^--Cu_2O buffers were deposited for 100 s, the p-Cu_2O/n-Cu_2O/ZnO and p-Cu_2O/p^--Cu_2O/ZnO devices varied significantly. The device containing a thin p^--Cu_2O layer exhibited a higher efficiency than did the device containing a thin n-Cu_2O layer. The apparent difference between V_{oc} for the p^--Cu_2O case (0.31 V) and the n-Cu_2O case (0.12 V) is at its greatest at this deposition time. The lower V_{oc} obtained for the p-Cu_2O/n-Cu_2O/ZnO device was due to the change in the morphology of the n-Cu_2O/ZnO interface during ECD processing at 100 s (Fig. 3b). During n-Cu_2O deposition, ZnO flakes formed on the ZnO film, damaging the p–n junction in the device. Current leakage occurred as observed in the dark *I–V* curve distribution as illustrated in Fig. 4b. In contrast, the interface between p^--Cu_2O and ZnO layers remained intact after the deposition of p^--Cu_2O (Fig. 3c). The higher V_{oc} of the p-Cu_2O/p^--Cu_2O/ZnO device is ascribable to the formation of an effective p–n junction diode, as shown by the dark *I–V* curve in Fig. 5b. This is probably because the deposition of p^--Cu_2O on ZnO in an ECD solution with pH = 9 was less harmful to the ZnO surface [6]. The ZnO film was thus protected by a thin p^--Cu_2O for further deposition of p-Cu_2O in an ECD solution with pH = 11. These results indicate that thin n-Cu_2O and p^--Cu_2O buffer layers differ in their impacts on PV device performance.

The thickness of the buffer layers in PV devices greatly affects device performance [30]. The PV efficiencies peaked at deposition periods of 600 s and 900 s cases for p-Cu_2O/n-Cu_2O/ZnO (Table 1a), and p-Cu_2O/p^--Cu_2O/ZnO (Table 1b), respectively. SEM images of the layers of the PV devices corresponding to the maximum efficiencies were shown in Fig. 6. Figure 6a reveals each layer of the p-Cu_2O/n-Cu_2O/ZnO device. The n-Cu_2O and ZnO layers cannot be clearly distinguished because of the formation of ZnO flakes (Fig. 3b). The thicknesses of the layers in the p-Cu_2O/n-Cu_2O/ZnO are approximately 1500 nm (p-Cu_2O) and 500 nm (n-Cu_2O/ZnO). The layers of the optimal p-Cu_2O/p^--Cu_2O/ZnO are shown in Fig. 6b. The thicknesses of each layer of the device are approximately 1500 nm (p-Cu_2O), 660 nm (p^--Cu_2O), and 500 nm (ZnO), respectively. In both devices, all PV parameters peaked because of the presence of the buffer layer. One possible reason for this is that an effective p–n junction diode was formed for the optimal Cu_2O buffer for each device. The p–n junction causes a depletion region to form in the Cu_2O buffer between the ZnO and p-Cu_2O layers, where useful electron–hole pairs can be stimulated by incident light. The distribution of the depletion region in PV devices containing buffer layers differs from those of PV devices without buffer layers. The Photocurrent (J_{sc}) of the devices with buffer layers increased, likely because the stimulated electrons and holes could separate effectively, and avoid recombination, thus extending the carrier lifetime in the devices [39]. Consequently, PV device performance was enhanced. The present study demonstrates

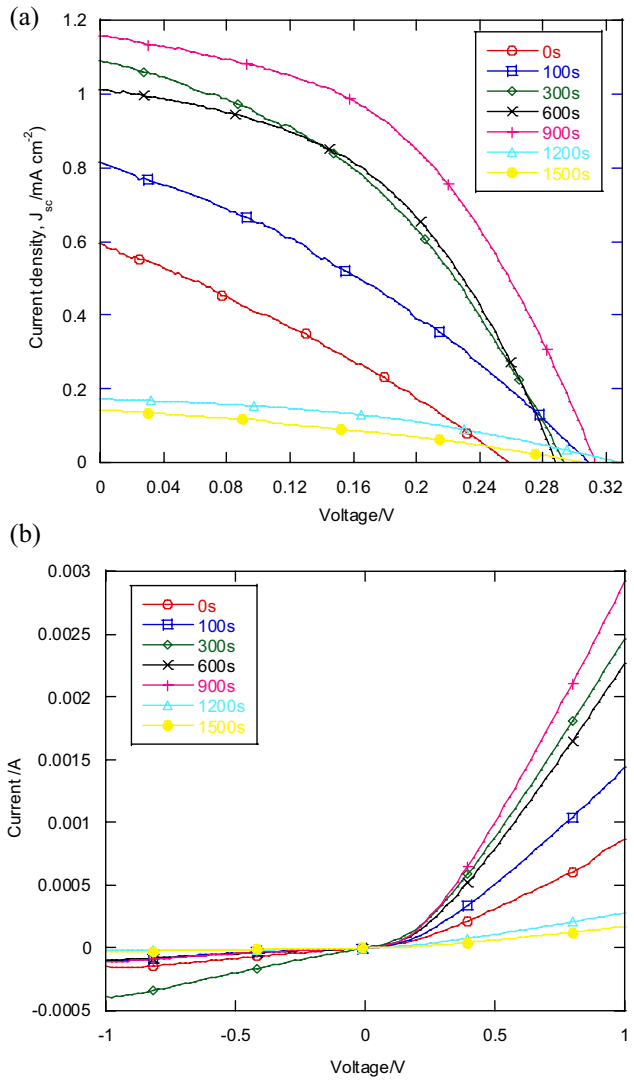

Fig. 5 Various deposition periods of p^{-}-Cu_2O in p-Cu_2O/p^{-}-Cu_2O/ZnO PV devices for **a** solar simulation and **b** dark *I–V* curve measurements

that the proper design and fabrication of a buffer layer in a p-Cu_2O/ZnO device can substantially enhance the PV device performance.

5 Conclusion

The design and fabrication of p-Cu_2O/n-Cu_2O/ZnO and p-Cu_2O/p^{-}-Cu_2O/ZnO PV devices was investigated through ECD techniques. Two types of buffer layers, n-Cu_2O and p^{-}-Cu_2O, were used to study the influence of buffer layers on PV device performance. The interface between the ZnO film and the Cu_2O buffer, and thickness of the buffer layer were identified as crucial determinants of PV device performance. The nanorod structure of the ZnO film transformed into flake-like structure when n-Cu_2O was deposited onto the ZnO film. By contrast, the nanorod structure of the ZnO film was maintained throughout the ECD of p^{-}-Cu_2O on ZnO. The optimal PV performance for both devices was achieved when the optimal thicknesses of the n-Cu_2O and p^{-}-Cu_2O buffer layers were obtained for their respective PV devices. The optimal efficiency of the PV devices was achieved through the fabrication and incorporation of Cu_2O buffers and enhanced from 0.046 (p-Cu_2O/ZnO) to 0.13% (p-Cu_2O/n-Cu_2O/ZnO) and 0.17% (p-Cu_2O/p^{-}-Cu_2O/ZnO).

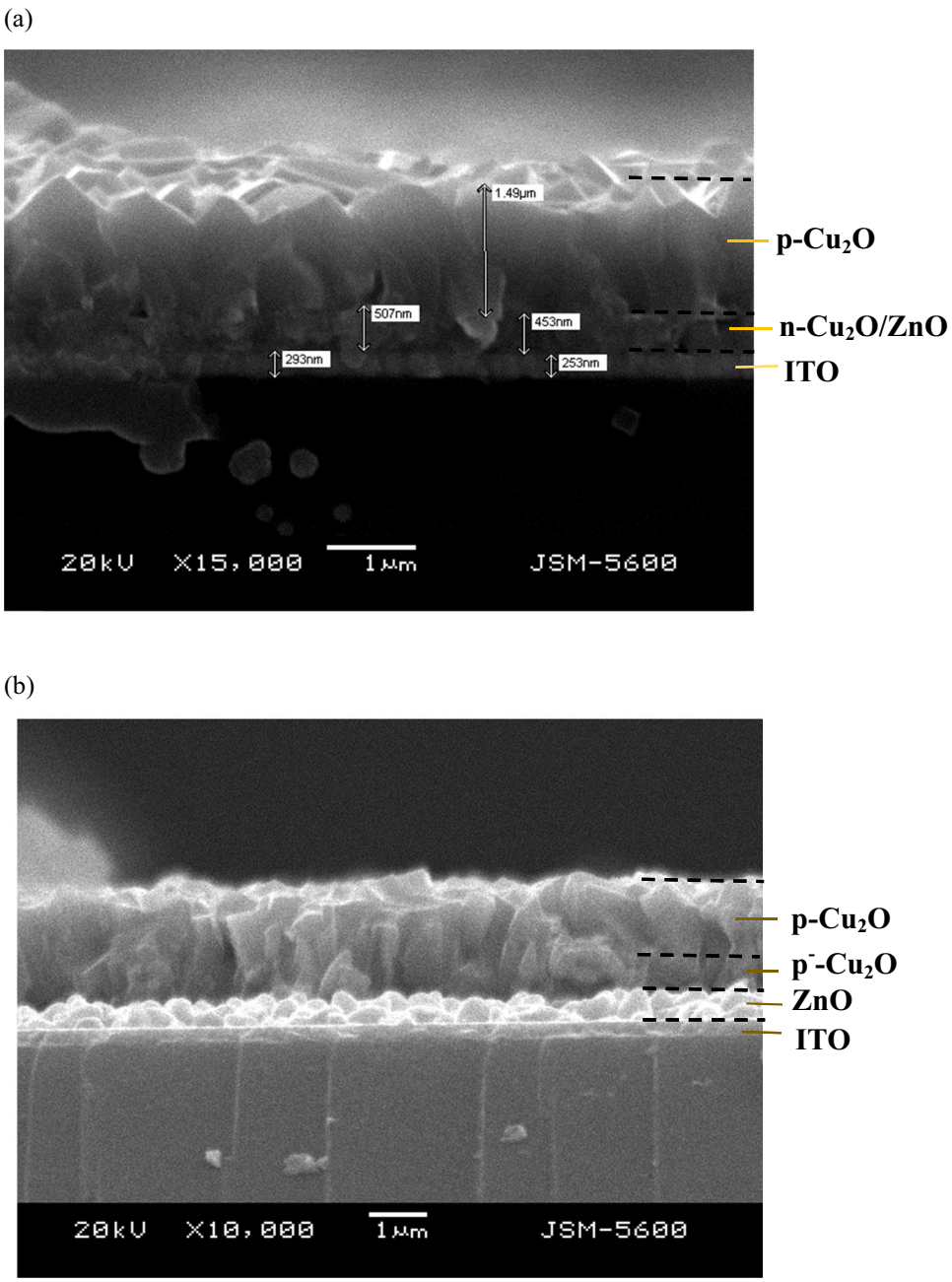

Fig. 6 SEM images of optimal thicknesses of Cu_2O buffer layers corresponding to the optimal efficiency in **a** p-Cu_2O/n-Cu_2O/ZnO, and **b** p-Cu_2O/p^--Cu_2O/ZnO PV devices

Acknowledgements This work is partially supported by the Ministry of Science and Technology, Taiwan, R.O.C. under Grant MOST 109-2221-E-155-047. The financial support is gratefully acknowledged.

References

1. Wick R, Tilley SD (2015) Photovoltaic and photoelectrochemical solar energy conversion with Cu_2O. J Phys Chem C 119:26243–26257
2. Ruhle S, Anderson AY, Barad HN, Kupfer B, Bouhadana Y, Rosh-Hodesh E, Zaban A (2012) All-oxide photovoltaics. J Phys Chem Lett 3:3755–3764
3. Jiang T, Xie T, Yang W, Chen L, Fan H, Wang D (2013) Photoelectrochemical and photovoltaic properties of p–n Cu_2O homojunction films and their photocatalytic performance. J Phys Chem C 117:4619–4624
4. Jin Z, Hu Z, Yu JC, Wang J (2016) Room temperature synthesis of a highly selective Cu/Cu_2O photocathode for photoelectrochemical water splitting. J Mater Chem A 4:13736–13741
5. Yoon J-S, Lee J-W, Sung Y-M (2019) Enhanced photoelectrochemical properties of Z-scheme ZnO/p-n Cu_2O PV-PEC cells. J Alloys Compd 771:869–876

6. Kang Z, Yan X, Wang Y, Bai Z, Liu Y, Zhang Z, Lin P, Zhang X, Yuan H, Zhang X, Zhang Y (2015) Electronic structure engineering of Cu_2O film/ZnO nanorods array all-oxide p-n heterostructure for enhanced photoelectrochemical property and self-powered biosensing application. Sci Rep 5:7882
7. Han K, Tao M (2009) Electrochemically deposited p-n homojunction cuprous oxide solar cells. Sol Energy Mater Sol Cells 93:153–157
8. Wei HM, Gong HB, Chen L, Zi M, Cao BQ (2012) Photovoltaic efficiency enhancement of Cu_2O solar cells achieved by controlling homojunction orientation and surface microstructure. J Phys Chem C 116:10510–10515
9. McShane CM, Choi KS (2012) Junction studies on electrochemically fabricated p-n Cu_2O homojunction solar cells for efficiency enhancement. Phys Chem Chem Phys 14:6112–6118
10. Zang Z (2018) Efficiency enhancement of ZnO/Cu_2O solar cells with well oriented and micrometer grain sized Cu2O films. Appl Phys Lett 112:042106
11. Jeong S, Song SH, Nagaich K, Campbell SA, Aydil ES (2011) An analysis of temperature dependent current-voltage characteristics of Cu_2O-ZnO heterojunction solar cells. Thin Solid Films 519:6613–6619
12. Hsueh T-J, Hsu C-L, Chang S-J, Guo P-W, Hsieh J-H, Chen I-C (2007) Cu_2O/n-ZnO nanowire solar cells on ZnO:Ga/glass templates. Scr Mater 57:53–56
13. Wong LM, Chiam SY, Huang JQ, Wang J, Pan JS, Chim WK (2010) Growth of Cu_2O on Ga-doped ZnO and their interface energy alignment for thin film solar cells. J Appl Phys 108:033702
14. Akimoto K, Ishizuka S, Yanagita M, Nawa Y, Paul GK, Sakurai T (2006) Thin film deposition of Cu_2O and application for solar cells. Sol Energy 80:715–722
15. Nishi Y, Miyata T, Minami T (2013) The impact of heterojunction formation temperature on obtainable conversion efficiency in n-ZnO/p-Cu_2O solar cells. Thin Solid Films 528:72–76
16. Ievskaya Y, Hoye RLZ, Sadhanala A, Musselman KP, MacManus-Driscoll JL (2015) Fabrication of ZnO/Cu_2O heterojunctions in atmospheric conditions: improved interface quality and solar cell performance. Sol Energy Mater Sol Cells 135:43–48
17. Izaki M, Shinagawa T, Mizuno K-T, Ida Y, Inaba M, Tasaka A (2007) Electrochemically constructed p-Cu2O/n-ZnO heterojunction diode for photovoltaic device. J Phys D 40:3326–3329
18. Jeong SS, Mittiga A, Salza E, Masci A, Passerini S (2008) Electrodeposited ZnO/Cu_2O heterojunction solar cells. Electrochim Acta 53:2226–2231
19. Cui J, Gibson UJ (2010) Simple two-Step electrodeposition of Cu_2O/ZnO nanopillar solar cells. J Phys Chem C 114:6408–6412
20. Hussain S, Cao C, Nabi G, Khan WS, Usman Z, Mahmood T (2011) Effect of electrodeposition and annealing of ZnO on optical and photovoltaic properties of the p-Cu_2O/n-ZnO solar cells. Electrochim Acta 56:8342–8346
21. Wei H, Gong H, Wang Y, Hu X, Chen L, Xu H, Liub P, Cao B (2011) Three kinds of Cu_2O/ZnO heterostructure solar cells fabricated with electrochemical deposition and their structure-related photovoltaic properties. Cryst Eng Comm 13:6065–6064
22. Hsu Y, Lina H, Chen M, Chen Y, Linc Y (2014) Polarity-dependant performance of p-Cu_2O/n-ZnO heterojunction solar cells. Electrochim Acta 144:295–299
23. Chen S, Lin L, Liu J, Lv P, Wu X, Zheng W, Qu Y, Lai F (2015) An electrochemical constructed p-Cu_2O/n-ZnO heterojunction for solar cell. J Alloys Compd 644:378–382
24. Abd-Ellah M, Thomas JP, Zhang L, Leung KT (2016) Enhancement of solar cell performance of p-Cu_2O/n-ZnO-nanotube and nanorod heterojunction devices. Sol Energy Mater Sol Cells 152:87–93
25. Zhu C, Panzer MJ (2015) Synthesis of Zn:Cu_2O thin films using a single step electrodeposition for photovoltaic applications. ACS Appl Mater Interfaces 7:5624–5628
26. Perng DC, Hong MH, Chen KH, Chen KH (2017) Enhancement of short-circuit current density in Cu_2O/ZnO heterojunction solar cells. J Alloys Compd 695:549–554
27. Fujimoto K, Oku T, Akiyama T (2013) Fabrication and characterization of ZnO/Cu_2O solar cells prepared by electrodeposition. Appl Phys Express 6:086503
28. Rosas-Laverde NM, Pruna A, Busquets-Mataix D, Mari B, Cembrero J, Salas Vicente F, Orozco-Messana J (2018) Improving the properties of Cu_2O/ZnO heterojunction for photovoltaic application by graphene oxide. Ceram Int 44:23045–23051
29. Nishi Y, Miyata T, Minami T (2016) Electrochemically deposited Cu_2O thin films on thermally oxidized Cu_2O sheets for solar cell applications. Sol Energy Mater Sol Cells 155:405–410
30. Lahmar H, Azizi A, Schmerber G, Dinia A (2016) Effect of the thickness of the ZnO buffer layer on the properties of electrodeposited p-Cu2O/n-ZnO/n-AZO heterojunctions. RSC Adv 6:68663
31. Marin AT, Muñoz-Rojas D, Iza DC, Gershon T, Musselman KP, MacManus-Driscoll JL (2013) Novel atmospheric growth technique to improve both light absorption and charge collection in ZnO/Cu_2O thin film solar cells. Adv Funct Mater 23:3413–3419
32. Fara L, Chilibon I, Nordseth Ø, Craciunescu D, Savastru D, Vasiliu C, Baschir L, Fara S, Kumar R, Monakhov E, Connolly JP (2020) Complex investigation of high efficiency and reliable heterojunction solar cell based on an improved Cu_2O absorber layer. Energies 13:4667
33. Yang T, Liu X, Din Y, Zhao S, Yin N (2018) Nondestructive interface construction for CdS-buffered ZnO nanorod/Cu_2O composite structure solar cells. J Nanopart Res 20:207
34. Fentahun DA, Tyagi A, Kar KK (2021) Numerically investigating the AZO/Cu_2O heterojunction solar cell using ZnO/CdS buffer layer. Optik 228:166228
35. Hsu CH, Chen LC, Lin YF (2013) Preparation and optoelectronic characteristics of ZnO/CuO-Cu_2O complex inverse heterostructure with GaP buffer for solar cell applications. Materials 6:4479–4488
36. Niu W, Zhou M, Ye Z, Zhu L (2016) Photoresponse enhancement of Cu_2O solar cell with sulfur-doped ZnO buffer layer to mediate the interfacial band alignment. Sol Energy Mater Sol Cells 144:717–723
37. Liau LCK, Tseng PC (2015) Effect of current pulse on electronic properties of Cu_2O films fabricated by electrochemical deposition process. Electrochim Acta 182:781–788
38. Liau LCK, Kuo PW (2020) Characterization of ZnO-Cu2O crystal films by electrochemical codeposition. J Solid State Electrochem 24:421–429
39. Neamen DA (2011) Semiconductor physics and devices. McGraw-Hill Higher Education, New York